

Hydroxyl as a Tracer of H₂ in the Envelope of MBM40

David L. Cotten and Loris Magnani

Department of Physics and Astronomy, University of Georgia, Athens, GA, 30602

dcotte1@physast.uga.edu, loris@physast.uga.edu

Elizabeth A. Wennerstrom

Wayne State University School of Medicine, Detroit, MI, 48201

Kevin A. Douglas

Department of Physics and Astronomy, University of Calgary, Calgary, Alberta

Joseph S. Onello

Department of Mathematical Sciences, The University of Montana, Missoula, MT, 59812-0864

Received _____; accepted _____

ABSTRACT

We observed 51 positions in the OH 1667 MHz main line transitions in the translucent high latitude cloud MBM40. We detected OH emission in 8 out of 8 positions in the molecular core of the cloud and 24 out of 43 in the surrounding, lower extinction envelope and periphery of the cloud. Using a linear relationship between the integrated OH line intensity and $E(B-V)$, we estimate the mass in the core, the envelope, and the periphery of the cloud to be 4, 8, and 5 M_{\odot} . As much as a third of the total cloud mass may be found in the periphery ($E(B-V) < 0.12$ mag) and about a half in the envelope ($0.12 \leq E(B-V) \leq 0.17$ mag). If these results are applicable to other translucent clouds, then the OH 1667 MHz line is an excellent tracer of gas in very low extinction regions and high-sensitivity mapping of the envelopes of translucent molecular clouds may reveal the presence of significant quantities of molecular mass.

Subject headings: ISM:molecules, ISM:clouds, ISM:abundances

1. Introduction

Most studies of molecular clouds have focused on the dense core regions where star formation is likely to occur (Blitz & Williams 1999; Bergin & Tafalla 2007). The surrounding, lower density, outer regions are less often studied because of the significantly weaker molecular lines and lack of star forming potential. However, this outer region is key for understanding the atomic-molecular interface in interstellar clouds and, possibly, their origin from the surrounding atomic interstellar medium (ISM). A standard way to categorize the smaller molecular clouds (in contrast to Giant Molecular Clouds which have masses $\geq 10^4 M_{\odot}$) was proposed by van Dishoeck & Black (1988) using visual extinction, A_V , to break up clouds into diffuse ($A_V < 1$ mag), translucent ($1 \leq A_V \leq 5$ mag), and dark ($A_V > 5$ mag) categories. Translucent molecular clouds are relatively easy to detect and map in the CO(J=1-0) transition and represent the vast majority of the high-latitude molecular clouds (Magnani et al. 1985, hereafter MBM). In contrast to dark molecular clouds which have dense, opaque cores surrounded by lower density, lower extinction “envelope” regions, translucent clouds are mostly “envelope”, at least in terms of spatial extent.

Translucent molecular clouds also differ significantly from dense, dark clouds in that translucent clouds are often not gravitationally bound. Consequently, their star-forming capability is either significantly less than that of dark clouds or, perhaps, non-existent (Hearty et al. 1999; McGehee 2008). Moreover, the way they form from the atomic ISM is also likely to be different from dark clouds and Bok globules. Some recent ideas invoke formation mechanisms for translucent clouds via shear flows or in regions where two HI velocity components meet (Shore et al. 2003; Barriault et al. 2010a). Thus, probing the atomic/molecular transition region is especially important for understanding the origin of translucent clouds.

Traditionally, the physical properties of molecular clouds are determined mainly by using the CO(1-0) line. Because of the mechanisms that destroy CO, it is possible that a regime of molecular gas exists where CO does not effectively trace the molecular content of the clouds

(van Dishoeck & Black 1988; Magnani & Onello 1993; Wannier et al. 1993; Grenier et al. 2005; Douglas & Taylor 2007; Barriault et al. 2010b). This regime is usually a region of very low dust column density surrounding the denser, more opaque cores, with the traditional threshold for sufficient obscuration to produce readily observable molecular lines in emission set at about $A_V \sim 1$ mag (van Dishoeck & Black 1988). However, recent work (Chastain et al. 2006; Barriault et al. 2010a) indicates that the CO(1-0) line can be readily detected down to $A_V \sim 0.3$ mag. This is significant because it forces a revision in both models of photodissociation regions (PDRs) and in molecular mass estimates for molecular clouds, and it provides the capability to study spectroscopically the transition region between the molecular cloud and the surrounding HI flows (see, e.g. Wannier et al. 1993; Barriault et al. 2010a).

Although the CO(1-0) transition is, historically, the one most commonly used to trace low-density, low-extinction gas, there are at least four other molecular and atomic species with transitions that have been used to trace gas at the edges of cloud cores in the so-called “envelope” region of a molecular cloud:¹ (1) The $^2\Pi_{3/2}$ OH ground state main lines at 1665 and 1667 MHz (Wannier et al. 1993; Wouterloot 1981; Liszt & Lucas 1996); (2) the $^2\Pi_{1/2}$ CH ground state main line at 3335 MHz (Magnani & Onello 1993); (3) the ortho $1_{10} - 1_{01}$ and para $2_{20} - 2_{11}$ transitions of C_3H_2 at 18.3 and 21.6 GHz (Cox et al. 1989); (4) the $^3P_1 \rightarrow ^3P_0$ fine structure line of atomic carbon at 492 GHz (Ingalls et al. 1997). All of these transitions have been proposed as potential tracers of H_2 in regions where the CO(1-0) line is not detectable (however, see Cotten & Magnani 2012, who claim that CO(1-0) observations at higher sensitivity than the usual 0.1 - 0.2 K rms can trace molecular gas in regions with A_V as low as 0.3 mag). Of the low-density tracers apart from CO, the OH main lines are the easiest to observe; they are readily detectable

¹In terms of the PDR models of atomic-molecular cloud interfaces, we are talking about the region where the carbon transitions from being primarily in the form of CI to that of CO (see, e.g., Hollenbach & Tielens 1997).

in translucent molecular clouds (Magnani et al. 1988; Magnani & Siskind 1990; Barriault et al. 2010b), OH is considered a precursor molecule to the formation of CO (e.g., Black & Dalgarno 1977), and thus from chemical considerations may be abundant in regions where the CO/H₂ abundance is low.

Previous CO(1-0) maps of MBM40 have focused primarily on the relatively dense, wishbone-shaped core region (Shore et al. 2003). In contrast, we studied the molecular envelope of this translucent cloud where the visual extinction is likely to be 0.3-0.5 mag (see below). CO(1-0) observations of this region require integration times of at least 15-20 minutes per position to reach rms values sufficiently low to detect lines in the envelope of this cloud (Cotten & Magnani 2012, in preparation). Moreover, the resolution of most millimeter wave, single-dish telescopes in North America is too high to allow systematic mapping of the extended envelope regions at sufficient sensitivity during typical observing runs. Observations of the CH and C₃H₂ lines described above require very long integrations, and the CI 492 GHz transition is difficult to observe from the ground. Thus, for these reasons, we surveyed the two OH main-line transitions in the envelope region of the translucent cloud MBM40. By using these observations to estimate the mass in the envelope and periphery regions of MBM40 we can compare how much molecular mass is tied up there that is not well-traced by traditional CO observational techniques. We discuss the translucent cloud selected for this study, MBM40, in Section 2 and describe our OH observations in Section 3. In Section 4 we discuss the W(OH) - E(B-V) relationship, the mass of OH in the cloud, and the molecular mass of the core and outer regions. The conclusions are summarized in section 5.

2. The Translucent Cloud MBM40

MBM40 is a small (≈ 2 square degrees), low extinction ($A_V \leq 3$ mag) cloud located at $\ell = 37.6^\circ$ and $b = 44.7^\circ$ that has been partially mapped in CO, ¹³CO, CS, H₂CO, CH and HI

(see Shore et al. 2003, for references). Figure 1 shows the IRIS² 100 micron emission for a $4^\circ \times 4^\circ$ region centered on the cloud. Clearly, there is significant dust emission surrounding the intense central core region (and associated smaller clouds to the east and west). A detailed CO(1-0) map of the horseshoe-shaped central region of the cloud with an rms sensitivity of 0.7 K was made by Shore et al. (2003). The horseshoe-like shape of this region will be referred to as the “core” of the cloud and CO(1-0) contours superposed on an E(B-V) map are shown in Figure 10 of Chastain et al. (2010). Although the Chastain et al. (2010) CO map effectively traces only the horseshoe or wishbone shaped core region, more sensitive CO integrations reveal CO(1-0) emission in the envelope region surrounding the core of the cloud (deVries 1988; Cotten & Magnani 2012, in preparation). We note that Wennerstrom (2007) also demonstrated that the 18 cm OH main lines could be detected from the envelope region of this cloud.

Chastain et al. (2006) showed that there is a marked increase in CO(1-0) detections for high-latitude regions with $E(B-V) \geq 0.12$ mag, so we divided MBM40 into three regions based on the E(B-V) maps by Schlegel et al. (1998, hereafter SFD). The three regions: $E(B-V) < 0.12$ mag, $0.12 \leq E(B-V) \leq 0.17$, and $E(B-V) > 0.17$, will be referred to as the “periphery”, the “envelope”, and the “core” respectively, throughout the rest of this paper. Of the roughly 2 square degrees that encompass the dust structure associated with MBM40, the periphery, envelope, and core regions cover 1.2, 0.61, and 0.20 square degrees, respectively.

3. Observations

Observations of the 18 cm ground state transitions of OH in MBM40 were made using the Robert C. Byrd 100 m radio telescope (hereafter GBT) in Green Bank, WV, during December

²IRIS are the new generation of IRAS images which benefit from improved zodiacal light subtraction, calibration, and destriping (Miville-Deschênes & Lagache 2005).

2009 and January 2010.³ The data were collected with the GBT using position switching with the “off” source position chosen to be between 1 and 2 degrees away from the “on” position, with exact locations based on the lowest emission region in the SFD-dust maps that allowed for slewing the telescope in azimuth only. All scans for a given position were averaged and a second order baseline was subtracted. A Gaussian curve was fit to each line, establishing values for the full width half maximum (FWHM), local standard of rest (LSR) centroid velocity, and peak temperature.

The spectra obtained from the GBT were produced using an autocorrelator spectrometer subdivided into four sections centered on the four 18 cm transitions at 1720.5300, 1667.3590, 1665.4018, and 1612.2310 MHz. However, given our integration times (typically half an hour per point) the satellite lines were so weak that they were not detected at all and even the 1665 MHz line had poor signal to noise for most lines of sight. Consequently, we focused our analysis only on the strongest line at 1667 MHz.⁴ For each scan two circular polarizations were measured but were averaged to produce a single spectrum. The bandwidth of each spectrum was 12.5 MHz, which corresponds to a velocity range of 2249 km s⁻¹ for the 1667 MHz line, and 2252 km s⁻¹ for the 1665 MHz line. The velocity resolution of each channel was 0.059 km s⁻¹. At 1667 MHz, the GBT has an angular resolution of 6.2 arc minutes and a beam efficiency of 1.32 times the aperture efficiency which is defined as the ratio of effective collecting area to physical collecting area, depending on the telescope geometry and on the frequency being observed. For observations at 18 cm the aperture efficiency is approximately 0.71, which corresponds to a beam efficiency of 0.94 at 18 cm. The radiation temperature, T_R , is thus $T_A/0.94$ (Maddalena 2009) where T_A is the

³The GBT is part of The National Radio Astronomy Observatory (NRAO) and is a facility of the National Science Foundation operated under cooperative agreement by Associated Universities, Inc. (www.gb.nrao.edu).

⁴In thermal equilibrium, the ratio of the 1667:1665:1720:1612 line intensity is 9:5:1:1.

antenna temperature.

Due to the long integration times needed to detect OH in low extinction regions, data from this work were combined with similar observations done by Wennerstrom (2007) in order to compile a larger data set for analysis. Figure 2 shows the SFD dust map for MBM40 overlaid with the positions of observations from this work (circles) and from Wennerstrom (2007) (squares). The earlier observations were conducted during the months of July and August in 2006 using the GBT in position switching mode, with the same basic setup and “off” position criteria used in this work. The combined data resulted in 3 detections out of 18 in the periphery region, 21 out of 25 in the envelope and 8 out of 8 in the core regions. The results of the observations for the 1667 MHz transition are given in Table 1 where the first two columns give the R.A. and Dec of each observation in J2000 coordinates, while the next three columns list the peak antenna temperature, the LSR centroid velocity, and the FWHM from a Gaussian fit to the profile. Column six tabulates $W(\text{OH})^5$; but if only one number is tabulated then that is the $1-\sigma$ upper limit of that specific observation. This upper limit is calculated by using the rms value of that specific observation as the temperature in conjunction with the average FWHM from all observations. The last column lists $E(\text{B-V})$ from the SFD database in magnitudes. The uncertainty in this quantity is $\sim 10\%$ (Schlegel et al. 1998).

4. Analysis

4.1. $W(\text{OH})$ - $E(\text{B-V})$ Relation

In Figure 3 all the $W(\text{OH})$ detections from Table 1 are plotted versus their associated $E(\text{B-V})$ value from the SFD database, and a line is fit to the data. Non-detections are also plotted as $1-\sigma$

⁵ $W(\text{OH}) = \int T_{\text{R}} dv$ with units of K km s^{-1} .

upper limits. The beam size of the OH observations (6.2') is nearly identical to the resolution of the SFD E(B-V) data (6.1'). The E(B-V) value has been corrected for the dust associated with atomic hydrogen in MBM40. This was done using HI data from Gir et al. (1994) to estimate N(HI) over a 3 km s^{-1} range centered on the cloud CO velocity. Shore et al. (2003) showed that HI emission over this range is directly associated with the molecular cloud. The N(HI) value associated with the cloud is converted to E(B-V) using the Bohlin et al. (1978) conversion factor. The HI correction only slightly changes the overall E(B-V) value, on average 0.018 mag, because most of the cloud has relatively low N(HI) values $\sim 1 \times 10^{20} \text{ (cm}^{-2}\text{)}$ compared to N(H₂) (see Chastain 2008). We will refer to that portion of the overall E(B-V) that is associated with molecular gas as E(B-V)_{H₂}. The linear relationship between W(OH)₁₆₆₇ and E(B-V)_{H₂} found using a least squares fit is

$$W(\text{OH})_{1667} = (0.71 \pm 0.08)E(\text{B} - \text{V})_{\text{H}_2} - 0.05 \pm 0.01 \text{ (K km s}^{-1}\text{)} \quad (1)$$

where E(B-V)_{H₂} is in magnitudes. The best fit line applies only to positions with detections in W(OH) and has a correlation coefficient of 0.78. Positions where W(OH) was not detected are labeled with arrows representing upper limits. A survival analysis was done including the non-detections to determine if a linear relationship could be assumed including the left-censored data. Including both censored and non-censored data a p value of 1.1×10^{-5} was obtained indicating that the variables are dependent on each other. Treating the OH upper limits as part of a bivariate censored problem, the Buckley-James method and the ASURV⁶ software package from Penn State University were used to calculate the linear relationship between all the W(OH)₁₆₆₇ and E(B-V) data:

⁶We used ASURV Rev. 1.2 ((LaValley et al. 1992)) which implements the methods presented by J(Isobe et al. 1986).

$$W(\text{OH})_{1667} = (0.54 \pm 0.12)E(\text{B} - \text{V})_{\text{H}_2} - 0.01 \quad (\text{K km s}^{-1}) \quad (2)$$

Since there are no heating sources in MBM40, the SFD dust map of the region is very similar to the IRIS 100 μm map. Thus, a linear relationship will also exist between $W(\text{OH})$ and the 100 μm radiance, as was found by Barriault et al. (2010b) and Grossman et al. (1990) for other translucent clouds. If we convert $E(\text{B}-\text{V})_{\text{H}_2}$ to visual extinction using the standard value for the optical total to selective extinction, and $W(\text{OH})$ to $N(\text{OH})$, we derive the OH/H_2 abundance (see section 4.3). The slope of the relationship shown in Figure 3 falls squarely on the median value from a compilation of primarily translucent lines of sight by Crutcher (1979) ($N(\text{OH})/A_V \approx 8 \times 10^{13} \text{ cm}^{-2} \text{ mag}^{-1}$).

Using the SFD dust map, $E(\text{B}-\text{V})_{\text{H}_2}$ values were found for all the SFD data points located in the three regions defined in Section 2, and from that, average $E(\text{B}-\text{V})_{\text{H}_2}$ values were calculated. We then used the relationship in Equation 2 to calculate an average $W(\text{OH})$ for the three extinction regimes (see Table 2). From this average $W(\text{OH})$ value, the area covered by each region, and the ratio of detections to observations, the total mass of OH in the cloud, M_{OH} , can be calculated, as described in the next section.

4.2. The OH Column Density and Mass

To obtain a mass for MBM40 we need the distance to the cloud. Welty et al. (1989) used echelle spectra near the Na I D lines to set an upper limit on the distance of ≤ 140 pc. In 1993, Penprase revised the distance of MBM40 to between 60 and 290 pc using Na I absorption of stars behind the cloud, and to $90 < d < 150$ pc by using CH observations. This improved estimate over the work by Welty et al. (1989) was due to additional foreground stars used to obtain a lower limit to the distance of MBM40. For this work we have adopted a distance of 120 pc which allows us

to calculate the cloud OH mass using:

$$M_{\text{OH}} = 4.14 \times 10^{-23} N(\text{OH}) \Omega d^2 (M_{\odot}) \quad (3)$$

where $N(\text{OH})$ is the average column density in cm^{-2} over the region, Ω is the solid angle covered by the region in question in square degrees, and d is the distance to the cloud in pc. For the column density, we use the formulation described by Wouterloot (1981):

$$N(\text{OH}) = 2.39 \times 10^{14} T_{\text{ex}} \Delta v \tau (\text{cm}^{-2}) \quad (4)$$

where T_{ex} is the excitation temperature of the transition, Δv is the FWHM of the line, and τ is the optical depth. In the optically thin approximation, the radiation temperature is related to optical depth by:

$$T_{\text{R}} = (T_{\text{ex}} - T_{\text{BG}}) \tau_{\nu} (\text{K}) \quad (5)$$

where T_{BG} is the background temperature at 18 cm: 3.3 K (e.g. Barriault et al. 2010b). Since we do not have an independent estimate of T_{ex} , we determined $N(\text{OH})$ for three plausible values of T_{ex} : 5, 10, and 20 K (Wouterloot 1981; Liszt & Lucas 1996; Harju et al. 2000). $N(\text{OH})$ values ranging from 9.4×10^{12} to $5.8 \times 10^{13} \text{ cm}^{-2}$ were obtained for the three temperature estimates. Average values of 1.2×10^{13} , 2.1×10^{13} , and $2.9 \times 10^{13} \text{ cm}^{-2}$ for the periphery, envelope, and core regions, respectively, were found for $T_{\text{ex}} = 10 \text{ K}$, and the mass of OH at that excitation temperature in the periphery, envelope, and core was 1.4×10^{-6} , 6.5×10^{-6} , and $3.5 \times 10^{-6} M_{\odot}$, respectively. For the other values of T_{ex} , the masses in the regions are shown in Table 3. In all cases, the OH mass in the envelope is greater than that in the core.

4.3. The OH Abundance and Molecular Mass in the Three Regions

To go from the OH mass to the overall molecular mass of the cloud, we must determine the value of the OH abundance with respect to H_2 . One of the earliest comprehensive astrochemical

models of translucent and diffuse molecular clouds with A_V ranging from 0.1 - 1 mag and T_K from 50 to 100 K was by Viala (1986), who found that the OH abundance with respect to H_2 varied from 3.8×10^{-9} to 9.4×10^{-9} . Another model by Nercessian et al. (1988) used the translucent cloud along the line of sight towards HD 29647 to calculate the OH abundance with respect to H_2 , and found that it varied from 2.6×10^{-8} to 1.2×10^{-6} depending on different heavy element depletions, cosmic ray ionization rates, and depth into the cloud. van Dishoeck & Black (1986) also calculated comprehensive models of diffuse and translucent clouds with 19 models where n_H ranged from 250 to 1000 cm^{-3} and T_K ranged from 20 to 100 K, yielding OH abundances ranging from 2.72×10^{-9} to 1.7×10^{-7} . Other OH abundance estimates were obtained for translucent clouds by van Dishoeck (1990) with values in the range 1.1×10^{-7} to 2.3×10^{-7} . Andersson & Wannier (1993) modeled the halo around dark molecular clouds, and obtained values for the OH abundance of $\sim 10^{-7}$. Empirically, Magnani et al. (1988) derived somewhat high OH abundances in the range 2×10^{-7} to 4×10^{-6} for a small sample of translucent clouds, and Weselak et al. (2010) obtained a value of $1.05 \pm 0.24 \times 10^{-7}$ from OH absorption line measurements of 5 translucent lines of sight; virtually identical to the analysis by Liszt & Lucas (2002). Because past studies have indicated that the OH abundance in lower density molecular regions can vary widely (4×10^{-9} to 1×10^{-6}), to determine the OH abundance in MBM40 we employ $E(B-V)$ as a surrogate for $N(H_2)$, and use our observations to provide $N(OH)$. In this manner a direct estimate of the OH/H_2 abundance in MBM40 can be obtained.

4.3.1. *The E(B-V) Method*

We obtain average OH/H_2 abundances for the 3 regions by using the well-established relationship between $H_{Total} = 2N(H_2) + N(HI)$ and $E(B-V)$ to determine H_2 (e.g. Bohlin et al. 1978). The $E(B-V)$ values used were found by averaging the SFD $E(B-V)$ values for each region. We can estimate $N(HI)$ for the lines of sight that we observed by using the HI map of MBM40

from Gir et al. (1994). In this manner we can determine $N(\text{H}_2)$ and, with the results of the previous section, the OH/H_2 abundance (see Table 4). The periphery, envelope, and the core have average values for the OH/H_2 abundance 3.0×10^{-7} , 1.1×10^{-6} , and 1.2×10^{-6} , respectively. We will use these values to go from the OH mass to the molecular mass.

4.3.2. *The Total Molecular Mass of the Core, Envelope, and Periphery*

Using the total OH mass of the cloud derived in Table 3 and the OH/H_2 abundance ratios from the previous section, we compute the total molecular mass of MBM40 for each region (see Table 5). Our results indicate that most of the mass of MBM 40 is contained in the envelope and periphery regions. The core may contain as little as 20% of the molecular mass of the cloud. The mass estimate for the core is actually an upper limit, since observations of the core in an optically thin line perforce include foreground and background envelope and periphery regions. For at least this cloud there is significant molecular gas contained outside of the regions mapped in CO using traditional “on the fly” mapping methods. If these results can be extrapolated to other clouds, then traditional CO(1-0) mapping of molecular clouds (i.e., with typical rms levels of 0.1 K) may not account for the bulk of the overall cloud molecular mass. This would be an important counterpoint to recent claims by Grenier et al. (2005) that half the molecular mass of the Galaxy may be “dark” in the sense of not traceable by radio spectroscopic means when CO and HI 21cm observations are considered. Our estimates of the M_{H_2} for the core region of MBM40 compares favorably with that of Chastain (2008) who derived a mass of $11 M_{\odot}$ from CO(1-0) observations.

5. Conclusions

High-sensitivity observations of the 1667 MHz OH line in the translucent cloud MBM40 enabled estimates of the molecular gas mass in its core, envelope, and periphery. Our focus was

the low extinction regions ($E(B-V) \leq 0.17$ mag) surrounding the CO-defined core region. From our analysis, we find that nearly half of the cloud’s molecular mass may reside in the envelope region surrounding the core, and we find that nearly a third of the molecular gas may reside in the periphery regions of the cloud where $E(B-V)$ is lower than 0.12 mag (equivalent to $A_V < 0.4$ mag). The core emission contains contributions from foreground and background gas in the envelope and periphery of the cloud. We have not attempted to correct the core mass for this so our results likely overestimate the contribution of the core to the overall cloud mass. The total molecular mass derived from our OH data is $17 M_\odot$ which compares favorably with the mass derived by Chastain (2008) from CO observations. A linear relationship between $W(\text{OH})$ and $E(B-V)$ exists for this cloud underscoring the efficacy of OH 1667 MHz observations in tracing low density molecular gas. OH emission is detected down to $E(B-V)$ level of 0.1 mag, corresponding to $A_V \sim 0.3$ mag. The OH 1667 MHz line is similar to the CO(1-0) line and the CH 3335 MHz line in tracing molecular emission at very low extinctions.

Our results confirm that there is significant mass in the regions surrounding the CO core of this translucent cloud. These regions are often at extinctions that were previously thought to be too low to contain enough molecular gas column density to be detected by radio spectroscopic emission lines. Results similar to ours have been established using CO data for the Taurus clouds by Goldsmith et al. (2008) and by Liszt and Pety (2012) for diffuse clouds. If OH does trace the envelope regions of translucent clouds, in general, then extensive high-sensitivity OH surveys of nearby molecular clouds should be undertaken to determine how much mass resides outside the traditionally CO-mapped cores.

This research was partially supported by the NRAO with the Student Observing Support Award (GSSP09-0018). The National Radio Astronomy Observatory is a facility of the National Science Foundation operated under cooperative agreement by Associated Universities, Inc.. This research has made use of the NASA/IPAC Infrared Science Archive, which is operated

by the Jet Propulsion Laboratory, California Institute of Technology, under contract with the National Aeronautics and Space Administration, and the ASURV statistical data analysis package from Penn State University. We would like to thank Ron Maddalena for help with the GBT observations. We would also like to thank Steve Shore and Harvey Liszt for a critical reading of the manuscript and an anonymous referee for several helpful suggestions especially regarding survival analysis of censored data.

REFERENCES

- Andersson, B.-G. & Wannier, P. G. 1993, *ApJ*, 402, 585
- Barriault, L., Joncas, G., Falgarone, E., & et al. 2010a, *MNRAS*, 406, 2713
- Barriault, L., Joncas, G., Lockman, F. J., & Martin, P. G. 2010b, *MNRAS*, 407, 2645
- Bergin, E. A. & Tafalla, M. 2007, *ARA&A*, 45, 339
- Black, J. H. & Dalgarno, A. 1977, *ApJS*, 34, 405
- Blitz, L. & Williams, J. P. 1999, *The Origin of Stars and Planetary Systems*. (Kluwer Academic Publishers)
- Bohlin, R., Savage, B., & Drake, J. 1978, *The Astrophysical Journal*, 224, 132
- Chastain, R. J. 2008, PhD thesis, The University of Georgia
- Chastain, R. J., Cotten, D. L., & Magnani, L. 2010, *ApJ*, 139, 267
- Chastain, R. J., Shelton, R. L., Raley, E. A., & Magnani, L. 2006, *AJ*, 132, 1964
- Cotten, D. L. & Magnani, L. 2012, in preparation
- Cox, P., Walmsley, C. M., & Guesten, R. 1989, *A&A*, 209, 382
- Crutcher, R. M. 1979, *ApJ*, 234, 881
- deVries, H. W. 1988, PhD thesis, Columbia University.
- Douglas, K. A. & Taylor, A. R. 2007, *ApJ*, 659, 426
- Gir, B., Blitz, L., & Magnani, L. 1994, *ApJ*, 434, 162
- Goldsmith, P. F., Heyer, M., Narayanan, G., et al. 2008, *ApJ*, 680, 428

Grenier, I. A., Casandjian, J. M., & Terrier, R. 2005, *Science*, 307, 1292

Grossman, V., Meyerdierks, H., Mebold, U., & Heitausen, A. 1990, *A&A*, 240, 400

Harju, J., Winnberg, A., & A., W. J. G. 2000, *A&A*, 353, 1065

Hearty, T., Magnani, L., Caillault, J.-P., et al. 1999, *A&A*, 341, 163

Hollenbach, D. J. & Tielens, A. G. G. M. 1997, *ARA&A*, 35, 179

Ingalls, J. G., Chamberlin, R. A., Bania, T. M., et al. 1997, *ApJ*, 479, 296

Isobe, T., Feigelsen, E., & Nelson, P. 1986, *ApJ*, 306, 490

LaValley, M., Isobe, T., & Feigelsen, E. 1992, *BAAS*, 24, 839

Liszt, H. & Lucas, R. 1996, *A&A*, 314, 917

Liszt, H. & Lucas, R. 2002, *A&A*, 384, 1054

Maddalena, R. 2009, *The Performance of the GBT A Guide for Planning Observations*,

<http://www.gb.nrao.edu/~rmaddale/GBT/ReceiverPerformance/PlaningObservations.htm>

Magnani, L., Blitz, L., & Mundy, L. 1985, *ApJ*, 295, 402

Magnani, L., Blitz, L., & Wouterloot, J. 1988, *ApJ*, 326, 909

Magnani, L. & Onello, J. S. 1993, *ApJ*, 408, 559

Magnani, L. & Siskind, L. 1990, *ApJ*, 359, 355

McGehee, P. M. 2008, *Handbook of Star Forming Regions, Volume II: The Southern Sky ASP Monograph Publications, Vol. 5 (B. Reipurth)*

Miville-Deschênes, M.-A. & Lagache, G. 2005, *ApJS*, 157, 302

- Nercessian, E., Benayoun, J. J., & Viala, Y. P. 1988, *A&A*, 195, 245
- Schlegel, D. J., Finkbeiner, D. P., & Davis, M. 1998, *ApJ*, 500, 525
- Shore, S. N., Magnani, L., LaRosa, T. N., & McCarthy, M. N. 2003, *ApJ*, 593, 413
- van Dishoeck, E. 1990, *PASP*, 12, 207
- van Dishoeck, E. F. & Black, J. H. 1986, *ApJS*, 62, 109
- van Dishoeck, E. F. & Black, J. H. 1988, *ApJ*, 334, 771
- Viala, Y. P. 1986, *A&AS*, 64, 391
- Wannier, P. G., Andersson, B.-G., Federman, S. R., et al. 1993, *ApJ*, 407, 163
- Welty, D. E., Hobbs, L. M., Blitz, L., & Penprase, B. E. 1989, *ApJ*, 346, 232
- Wennerstrom, E. 2007, Master's thesis, The University of Georgia
- Weselak, T., Galazutidinov, G. A., Beletsky, Y., & Krelowski, J. 2010, *MNRAS*, 402, 1991
- Wouterloot, J. 1981, PhD thesis, The University of Leiden: Leiden.

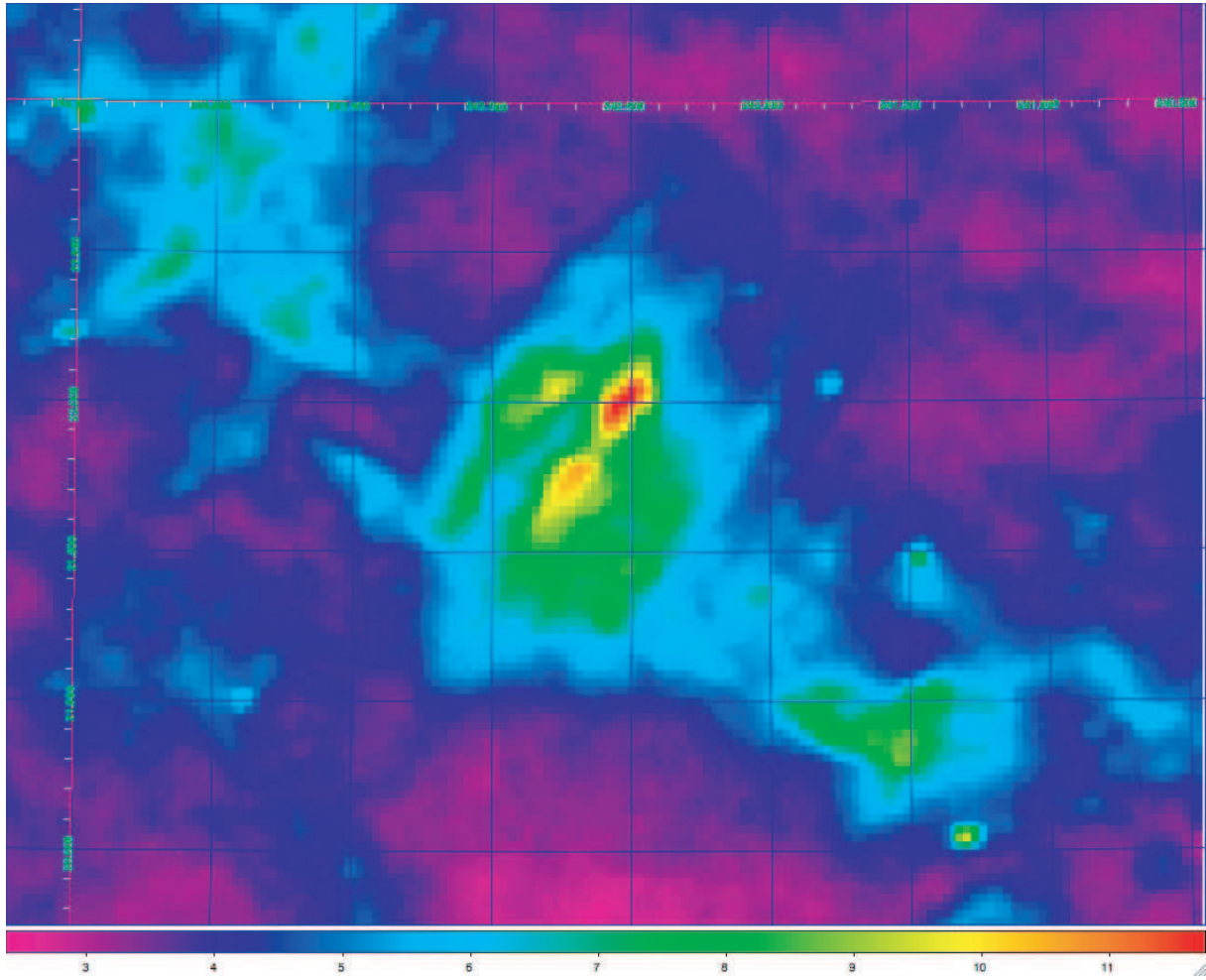


Fig. 1.— IRIS 100 micron emission map of MBM40 and its environs. The central brightest region shows the horse-shoe or hairpin structure mapped in CO(1-0) by Shore et al. (2003). The surrounding region is the “envelope” of the cloud. The dust structures to the northeast and southwest are probably related to MBM40 but have never been mapped in CO. The intensity scale is in MJy/ster.

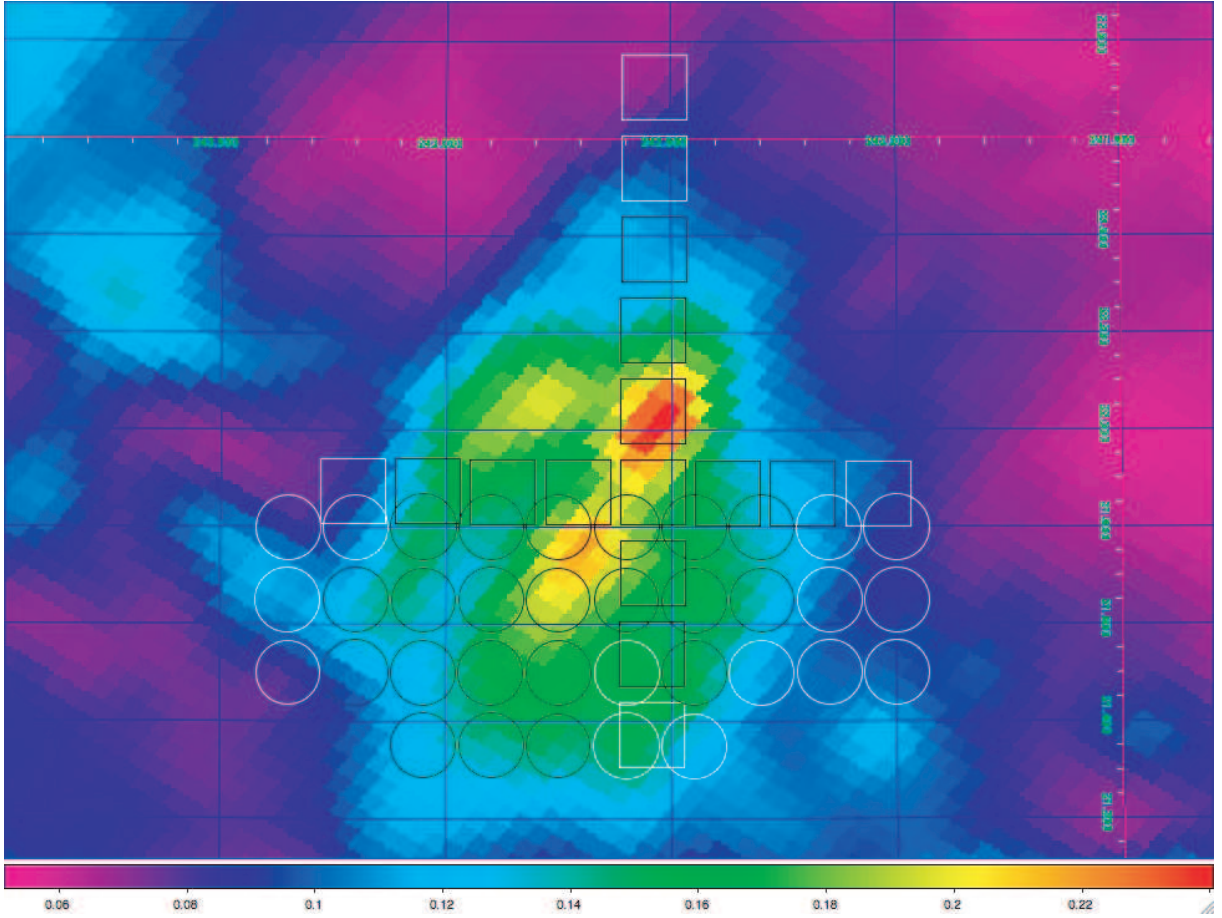


Fig. 2.— $E(B-V)$ map of MBM40 from the Schlegel, Finkbeiner, & Davis (1998), overlaid with OH observations of the 1667 MHz line from this work (circles) and from Wennerstrom (2007, squares). Detections are represented by black symbols, non detections by white symbols. See Table 1 for line parameters. The intensity scale is in MJy/ster.

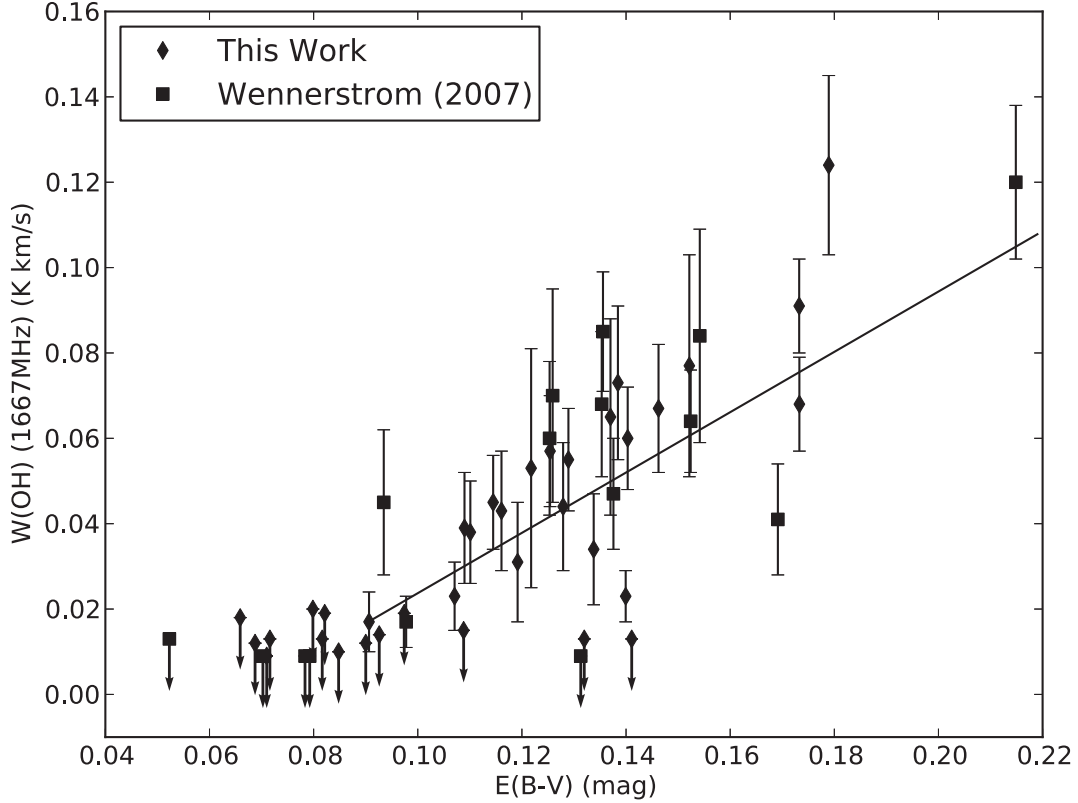


Fig. 3.— $W(OH)_{1667}$ in units of $(K \text{ km s}^{-1})$ versus $E(B-V)_{H_2}$ in (mag) for MBM40. The arrows represent upper limits for $W(OH)$. The least squares fit applies only to the points that are not upper limits. The resolution of the OH data and the $E(B-V)$ data from Schlegel et al. (1998) is nearly identical ($6.2'$ vs. $6.1'$), and the uncertainty in $E(B-V)$ is 10%.

Table 1. OH 1667 MHz observations in MBM40.

RA (2000) (deg)	Dec (2000) (deg)	T_A (K)	v_{LSR} (km s ⁻¹)	Δv (km s ⁻¹)	$W(OH)^a$ (K km s ⁻¹)	$E(B-V)_{H_2}^b$ (mag)
243.35	21.80				0.009	0.071
243.20	21.80				0.009	0.085
243.05	21.80	0.075 +/- 0.016	2.94	0.64 +/- 0.13	0.055 +/- 0.012	0.129
242.90	21.80	0.070 +/- 0.016	3.25	0.71 +/- 0.16	0.057 +/- 0.013	0.125
242.75	21.80	0.155 +/- 0.018	3.31	0.51 +/- 0.06	0.091 +/- 0.011	0.173
242.60	21.80	0.103 +/- 0.017	3.34	0.58 +/- 0.09	0.068 +/- 0.011	0.173
242.45	21.80	0.052 +/- 0.012	3.73	0.39 +/- 0.09	0.023 +/- 0.006	0.140
242.30	21.80	0.057 +/- 0.014	3.66	0.69 +/- 0.17	0.045 +/- 0.011	0.115
242.15	21.80				0.012	0.090
242.00	21.80				0.012	0.069
243.35	21.65				0.014	0.093
243.20	21.65	0.041 +/- 0.013	2.59	0.81 +/- 0.26	0.038 +/- 0.012	0.110
243.05	21.65	0.032 +/- 0.014	3.08	0.84 +/- 0.37	0.031 +/- 0.014	0.119
242.90	21.65	0.081 +/- 0.020	3.31	0.79 +/- 0.19	0.073 +/- 0.018	0.138
242.75	21.65	0.129 +/- 0.022	3.31	0.84 +/- 0.14	0.124 +/- 0.021	0.179
242.60	21.65	0.043 +/- 0.014	3.48	1.57 +/- 0.52	0.077 +/- 0.026	0.152
242.45	21.65	0.041 +/- 0.015	3.24	1.40 +/- 0.50	0.065 +/- 0.023	0.137
242.30	21.65	0.042 +/- 0.014	3.29	0.90 +/- 0.29	0.043 +/- 0.014	0.116
242.15	21.65				0.013	0.082
242.00	21.65				0.013	0.072

Table 1—Continued

RA (2000) (deg)	Dec (2000) (deg)	T_A (K)	v_{LSR} (km s ⁻¹)	Δv (km s ⁻¹)	$W(OH)^a$ (K km s ⁻¹)	$E(B-V)_{H_2}^b$ (mag)
243.35	21.50				0.018	0.066
243.20	21.50	0.033 +/- 0.014	2.59	0.46 +/- 0.19	0.017 +/- 0.007	0.091
243.05	21.50	0.049 +/- 0.016	3.32	0.69 +/- 0.23	0.039 +/- 0.013	0.109
242.90	21.50	0.083 +/- 0.016	3.32	0.63 +/- 0.12	0.060 +/- 0.012	0.140
242.75	21.50	0.075 +/- 0.016	3.55	0.77 +/- 0.17	0.067 +/- 0.015	0.146
242.60	21.50				0.013	0.141
242.45	21.50	0.037 +/- 0.014	3.20	0.80 +/- 0.30	0.034 +/- 0.013	0.134
242.30	21.50				0.019	0.097
242.15	21.50				0.019	0.082
242.00	21.50				0.020	0.080
243.05	21.35	0.061 +/- 0.020	3.02	0.34 +/- 0.11	0.023 +/- 0.008	0.107
242.90	21.35	0.036 +/- 0.019	3.42	1.30 +/- 0.67	0.053 +/- 0.028	0.122
242.75	21.35	0.051 +/- 0.017	3.19	0.75 +/- 0.25	0.044 +/- 0.015	0.128
242.60	21.35				0.013	0.132
242.45	21.35				0.015	0.109
Wennerstrom (2007) data						
242.54	21.87	0.050 +/- 0.016	3.25	0.71 +/- 0.22	0.041 +/- 0.013	0.169
242.54	22.03	0.123 +/- 0.018	2.96	0.85 +/- 0.12	0.120 +/- 0.018	0.215
242.53	22.20	0.107 +/- 0.018	3.06	0.69 +/- 0.11	0.085 +/- 0.014	0.136
242.53	22.37	0.044 +/- 0.017	3.47	0.88 +/- 0.34	0.045 +/- 0.017	0.093

Table 1—Continued

RA (2000) (deg)	Dec (2000) (deg)	T_A (K)	v_{LSR} (km s ⁻¹)	Δv (km s ⁻¹)	$W(OH)^a$ (K km s ⁻¹)	$E(B-V)_{H_2}^b$ (mag)
242.53	22.53				0.009	0.079
242.53	22.70				0.013	0.052
242.54	21.70	0.055 +/- 0.017	3.49	1.34 +/- 0.40	0.084 +/- 0.025	0.151
242.54	21.53	0.040 +/- 0.011	3.11	1.03 +/- 0.29	0.047 +/- 0.013	0.138
242.54	21.37				0.009	0.131
242.37	21.86	0.056 +/- 0.017	3.65	0.93 +/- 0.27	0.060 +/- 0.018	0.125
242.20	21.86	0.030 +/- 0.010	3.62	0.49 +/- 0.16	0.017 +/- 0.006	0.098
242.04	21.86				0.009	0.078
242.70	21.87	0.087 +/- 0.016	3.30	0.64 +/- 0.11	0.064 +/- 0.012	0.152
242.87	21.87	0.072 +/- 0.018	3.03	0.82 +/- 0.20	0.068 +/- 0.017	0.135
243.04	21.87	0.048 +/- 0.017	3.12	1.29 +/- 0.46	0.070 +/- 0.025	0.126
243.20	21.87				0.009	0.070

^aIf there is no error associated with the $W(OH)$ entry, then it is a $1-\sigma$ upper limit.

^b $E(B-V)_{H_2}$ is the color excess associated with the molecular gas in the cloud. The contribution from dust associated with HI has been subtracted.

Table 2. Average $E(B-V)_{H_2}$ and $W(OH)_{1667}$ values for the MBM40 regions (see Section 2).

Region	$E(B-V)_{H_2}$ (mag)	$W(OH)_{1667}$ (K km s ⁻¹)
Periphery	0.08	0.033
Envelope	0.13	0.060
Core	0.17	0.082

Table 3. Total $M(OH)$ for 3 regions in MBM40.

Region	detection fraction	$T_{ex} = 5$ K ($10^{-6}M_{\odot}$)	$T_{ex} = 10$ K ($10^{-6}M_{\odot}$)	$T_{ex} = 20$ K ($10^{-6}M_{\odot}$)
Periphery	0.17	2.8 ± 3.3	1.4 ± 1.7	0.6 ± 0.7
Envelope	0.84	12.9 ± 4.2	6.5 ± 2.3	5.2 ± 1.7
Core	1.0	6.9 ± 1.6	3.5 ± 0.9	2.8 ± 0.7

Table 4. OH/H_2 abundance ratio (10^{-7}) for 3 regions in MBM40.

Region	$T_{ex} = 5$ K	$T_{ex} = 10$ K	$T_{ex} = 20$ K	Average
Periphery	5.6 ± 3.4	2.3 ± 1.4	1.2 ± 0.7	3.0
Envelope	16.9 ± 4.7	8.5 ± 2.5	6.7 ± 1.9	10.9
Core	18.5 ± 3.9	9.6 ± 2.0	7.2 ± 1.5	11.8

Table 5. Total $M(\text{H}_2)$ for MBM40.

Region	Mass (M_{\odot})
Periphery	5.2 ± 6.3
Envelope	7.6 ± 2.5
Core	3.8 ± 0.9
Total	16.6 ± 9.7